

# Non-equilibrium Lattice-driven Dynamics of Stripes in Nickelates using Time-Resolved X-ray Scattering

W. S. Lee,<sup>1,\*</sup> Y. F. Kung,<sup>1,2</sup> B. Moritz,<sup>1,3,4</sup> G. Coslovich,<sup>5,6</sup> R. A. Kaindl,<sup>5</sup> Y. D. Chuang,<sup>7</sup> R. G. Moore,<sup>1</sup> D. H. Lu,<sup>8</sup> P. S. Kirchmann,<sup>1</sup> J. S. Robinson,<sup>5,6</sup> M. P. Miniti,<sup>6</sup> G. Dakovski,<sup>6</sup> W. F. Schlotter,<sup>6</sup> J. J. Turner,<sup>6</sup> S. Gerber,<sup>1</sup> T. Sasagawa,<sup>9</sup> Z. Hussain,<sup>10</sup> Z. X. Shen,<sup>1,†</sup> and T. P. Devereaux<sup>1,‡</sup>

<sup>1</sup>Stanford Institute for Materials and Energy Sciences,

SLAC National Accelerator Laboratory, Menlo Park, CA 94025, USA

<sup>2</sup>Department of Physics, Stanford University, Stanford, CA 94305, USA.

<sup>3</sup>Department of Physics and Astrophysics, University of North Dakota, Grand Forks, ND 58202, USA

<sup>4</sup>Department of Physics, Northern Illinois University, DeKalb, IL 60115, USA

<sup>5</sup>Materials Sciences Division, Lawrence Berkeley National Laboratory, Berkeley, CA 94720, USA

<sup>6</sup>Linac Coherent Light Source, SLAC National Accelerator Laboratory, Menlo Park, CA 94720, USA

<sup>7</sup>Advanced Light Source, Lawrence Berkeley National Laboratory, Berkeley, CA 94720, USA

<sup>8</sup>Stanford Synchrotron Radiation Lightsource, SLAC National Accelerator Laboratory, Menlo Park, CA, 94025, USA

<sup>9</sup>Materials and Structures Laboratory, Tokyo Institute of Technology, Kanagawa 226-8503, Japan

<sup>10</sup>Advanced Light Source, Lawrence Berkeley National Laboratory, Berkeley, CA 94720

(Dated: February 28, 2017)

We investigate the lattice coupling to the spin and charge orders in the striped nickelate,  $\text{La}_{1.75}\text{Sr}_{0.25}\text{NiO}_4$ , using time-resolved resonant x-ray scattering. Lattice-driven dynamics of both spin and charge orders are observed when the pump photon energy is tuned to that of an  $E_u$  bond-stretching phonon. We present a likely scenario for the behavior of the spin and charge order parameters and its implications using a Ginzburg-Landau theory.

PACS numbers: Valid PACS appear here

Strong correlations between spin, charge, lattice, and orbital degrees of freedom can lead to the emergence of quantum phases, in which electrons exhibit collective behaviors [1]. To manipulate and control these collective states, it is crucial to learn how they couple to underlying degrees of freedom that can be altered by external fields or perturbations. However, information about such collective coupling is largely unavailable. Theoretically, it is difficult to predict because the microscopic mechanisms underlying these collective phases are mostly unknown and their behavior is not captured well by theories based on effective single electron interactions. Experimentally, collective coupling has also proven to be elusive.

The stripe state in the nickelate  $\text{La}_{2-x}\text{Sr}_x\text{NiO}_4$  highlights this difficulty [2]. As illustrated in Fig. 1(a), doped holes segregate into periodically ordered charge stripes, serving as anti-phase domain walls for the antiferromagnetically ordered spin stripes [3–6]. The charge (CO) and spin orders (SO), which simultaneously break translational and rotational symmetry, are coupled [8, 28] and aligned along the “diagonal” direction, *i.e.*  $45^\circ$  with respect to the Ni-O bond direction. Some theories have argued that the formation of both SO and CO cannot be attributed solely to the Coulomb interactions between electrons [9, 10], which primarily stabilize the SO; coupling to the lattice degree of freedom should play an equally important role for CO.

A splitting of the bond-bending  $E_u$  phonons at the Brillouin zone center, which has been associated with the phonon Brillouin-zone-folding may hint at this kind

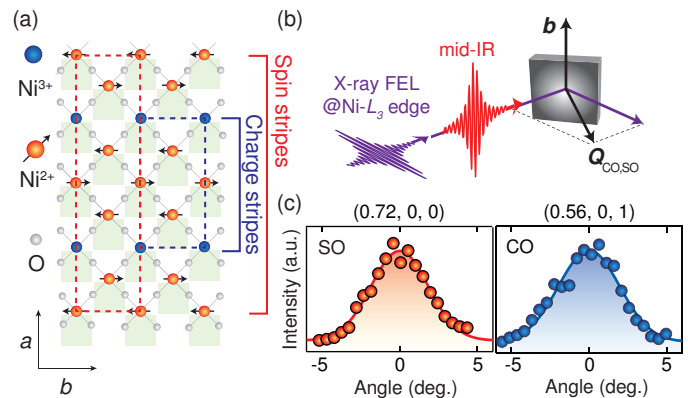


FIG. 1: (color online) (a) Stripe phase of  $\text{La}_{1.75}\text{Sr}_{0.25}\text{NiO}_4$ . The blue markers represent the doped holes that form the charge stripe order. The markers with arrows represent the direction of spins at Ni high spin sites ( $S = 1$ ), which give rise to the spin stripe order. The blue (red) dashed box indicates the period of the charge (spin) order. (b) The experimental setup is sketched in the top panel. (c) Diffraction peak profiles of SO and CO taken by rotating the sample angle (*i.e.* rocking curve) in the scattering plane under equilibrium condition (*i.e.* without laser pumping). The reciprocal positions of the peak position are indicated in the upper horizontal axis. The trajectories of the rocking curves in the reciprocal space are  $(0.717, 0, -0.15)$ - $(0.72, 0, 0)$ - $(0.717, 0, 0.15)$  and  $(0.52, 0, 1.11)$ - $(0.56, 0, 1)$ - $(0.6, 0, 0.88)$  for SO and CO, respectively.

of collective coupling [12]. However, such folding was not observed on another  $E_u$  bond-stretching phonon [13, 14], despite its unusual temperature dependence that was

attributed to the formation of short-range charge order [11, 14]. Moreover, a direct observation of collective coupling in momentum space is difficult. On one hand, lattice distortions due to the formation of charge stripes and lattice fluctuations associated with dynamical charge stripes have been observed [15], suggesting a collective coupling to CO. On the other hand, inelastic neutron scattering has revealed anomalies in the energy-momentum dispersion of bond-stretching phonons unrelated to both the wavevectors and temperature dependence of stripes [16]. This behavior contrasts with the classical charge density wave (CDW) systems arising from a Peierls transition, where phonons collectively couple to the CDW, causing an anomalous softening and broadening of the phonon spectra near the CDW wavevector [17, 18]. In addition, whether the lattice couples to the SO directly or parasitically via the CO remains an open question that is difficult to answer via conventional experimental probes.

To determine whether the lattice couples collectively to stripe order, we use a pump-probe approach to investigate the relationship between the lattice, SO, and CO. We tune the wavelength of a mid-infrared (IR) laser pulse to resonantly excite the bond-stretching  $E_u$  mode [19]. The dynamics of the SO and CO are directly recorded using time-resolved resonant x-ray scattering at the Ni  $L_3$ -edge with sub-picosecond resolution. Upon photoexcitation of the  $E_u$  phonon, both the SO and CO are suppressed immediately, initiating lattice-driven dynamics. Interestingly, the SO responds more strongly than the CO, in contrast to the case of non-resonant IR pumping [8]. This differs from the naive expectation that CO should couple more directly to phonons. Using a Ginzburg-Landau theory, we show that phonons should affect both CO and SO collective behavior.

Experiments were performed at the Soft X-ray Materials Science (SXR) instrument of the Linac Coherent Light Source (LCLS) [21] using the Resonant Soft X-ray Scattering (RSXS) Endstation [22]. Nickelate single crystals,  $\text{La}_{1.75}\text{Sr}_{0.25}\text{NiO}_4$ , with a doping level of  $x \sim 0.25$  were selected for the experiments. The SO and CO transition temperatures were approximately 100 K and 110 K, respectively [8]. All measurements were conducted at a temperature of 50 K, well below both the SO and CO transition temperatures. The experimental configuration is sketched in Fig. 1(b). The duration of the X-ray free electron laser (FEL) pulses was 40 fs with a beam spot of approximately 300  $\mu\text{m}$  in diameter. Intense tunable pump pulses were generated by driving an optical parametric amplifier (OPA) with a Ti:sapphire amplifier synchronized to the FEL, followed by difference frequency mixing in GaSe. The 0.8  $\mu\text{m}$  and 5  $\mu\text{m}$  laser pulses were sub-100 fs, while the 11  $\mu\text{m}$  and 14.7  $\mu\text{m}$  pulses were approximately 400 fs to minimize spectral overlap and maximize the resonant effect at the  $E_u$  mode energy. The dynamics of SO and CO were measured by

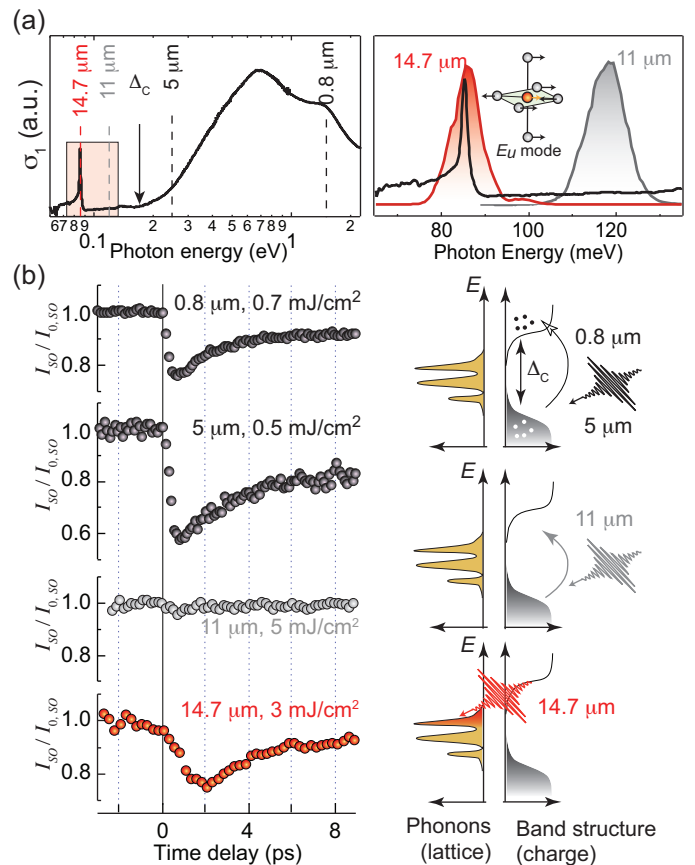


FIG. 2: (color online) (a) Real part of the optical conductivity  $\sigma_1$  of  $\text{La}_{1.75}\text{Sr}_{0.25}\text{NiO}_4$  taken at 50 K. An enlarged view of the red shaded area is plotted in the lower panel. The associated spectral bandwidths of the 14.7 (red) and 11  $\mu\text{m}$  (grey) pump laser pulses are also superimposed for comparisons. The eigen-motion of the  $E_u$  phonon is sketched in the lower panel. The charge gap  $\Delta_C$  is estimated to be the onset of optical conductivity at approximately 180 meV. (b) Time traces of normalized SO diffraction peak intensity taken with pump pulses of different wavelengths whose energies are also indicated in (a). The intensities are normalized to the average SO peak intensity before time zero,  $I_{0,\text{SO}}$ . Microscopic schematics of photo-excitations associated with different pump wavelengths are sketched on the right panels. The lattice degree of freedom and the electronic band structure are sketched separately, as denoted.

tracking the evolution of diffraction peak intensities as a function of the time delay between the optical pump and the XFEL pulses. The diffraction peak intensity was recorded by an avalanche photodiode (APD), positioned at the equilibrium diffraction peak position. The photon energy of the FEL pulse was tuned to the Ni  $L_3$ -edge with a bandwidth of 1 eV, allowing measurements of both the diffraction peaks of the SO and CO at  $Q_{\text{SO}} = (0.72, 0, 0)$  and  $Q_{\text{CO}} = (0.56, 0, 1)$  in reciprocal space, respectively [6, 8, 23] [see Fig. 1(c)]. Additional details about the experimental setup can be found in the Supplemental Material.

The real-part of the optical conductivity is shown in Fig. 2(a). The broad feature at higher energies arises from electronic interband dipole transitions. At energies below  $\sim 180$  meV, the spectral weight is strongly suppressed due to the presence of a charge gap  $\Delta_C$  [13], associated with changes in the hole transport that precede stripe formation [14]. At energies smaller than  $\Delta_C$ , a sharp spectral peak at 85 meV, associated with a bond-stretching  $E_u$  phonon, dominates the spectrum [14, 25]. It consists of shear motion of the oxygen atoms as illustrated in Fig. 2(a) [19]. Other IR-active phonons with lower energies exist, but are inaccessible with our setup and will not be discussed here.

Figure 2(b) shows the SO dynamics induced by the pump laser with different wavelengths (*i.e.* different pump photon energies). For the pump photon energy higher than  $\Delta_C$  (*e.g.* 0.8 and 5  $\mu\text{m}$ ), photo-excitation creates delocalized electrons with energies significantly higher than  $\Delta_C$  [14]. These “hot electrons” suppress both the SO and CO with a stronger effect on CO, as discussed in previous studies [8, 23]. Reducing the pump photon energy below  $\Delta_C$  changes the character of the dynamics. Suppression and dynamics of SO are negligible at 11  $\mu\text{m}$ , as photons cannot be absorbed due to the lack of electronic density of states inside the charge gap. When the pump photon energy coincides with the energy of the  $E_u$  phonon, *i.e.* 14.7  $\mu\text{m}$ , the SO dynamics reappears, although the pump cannot create “hot electrons” across the  $\Delta_C$  to suppress SO. Therefore, the observed dynamics must be induced by coupling to photo-excited lattice modes. We note that the time scale for the initial suppression is on the order of 2 - 3 ps, which cannot be accounted for by the longer pulse duration of the 14.7  $\mu\text{m}$  laser and the temporal resolution. Potentially, this is a characteristic of the lattice-driven SO dynamics, motivating future studies with higher precision to determine time-zero.

It is important to note that while we resonantly excite the  $E_u$  phonons at zero momentum transfer, other phonons can be generated through nonlinear processes. For example, bond-stretching phonons with finite momenta can be induced through multi-phonon processes that satisfy momentum conservation. In addition, nonlinear processes can also generate two symmetry-allowed  $A_{1g}$  Raman-active phonons with lower energies [15, 26], corresponding to the  $c$ -axis motions of the lanthanum and apical oxygen atoms. [19]. Thus, we cannot attribute the lattice-induced dynamics solely to the 14.7  $\mu\text{m}$   $E_u$  phonon. Nevertheless, the excitations can be attributed phenomenologically to some form of instantaneous lattice distortion, which couples to the collective stripe state.

Figure 3 shows the lattice-induced dynamics of both SO and CO. Interestingly, exciting the bond stretching  $E_u$  phonon suppresses the intensity of SO more than CO [Fig. 3(a)]. This contrasts to the expectation derived from the electron-phonon coupling picture, which would

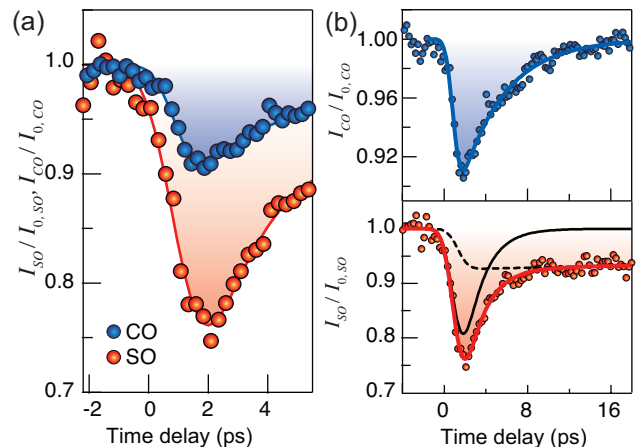


FIG. 3: (color online) (a) The response of the SO and CO induced by resonantly exciting the  $E_u$  phonons with 14.7  $\mu\text{m}$  laser pulses. Note that the same pump fluence is used for the two measurements. (b) Associated recovery dynamics of SO and CO at longer time. While the dynamics of CO can be described by a single time scale, SO dynamics contains an additional slow time scale, likely associated with spin-reorientation [8, 23]. The solid curves are single exponential fits of the relaxation time scale. The slow dynamics of SO is fit to a constant offset after time zero.

predict a stronger response for CO than SO. This also appears to differ from the case of “hot-electron” dynamics, where CO is affected more than SO [8, 23].

Note that instrumental limitations force us to measure the intensity change only at a single position in the Brillouin zone. Hence the time evolution of the diffraction peak profile (position and width) is unavailable to unambiguously determine the behaviors of the SO and CO order parameters, including their amplitude, periodicity, and correlation length, for the “lattice-driven”-dynamics. However, we argue that the periodicity of the order parameters is unlikely to change, as the mid-IR photo-excitation primarily excites phonons with zero momentum, whose eigen-motion is identical between unit cells and thus provides no driving force to change the ordering periodicity. In general, altering the SO and CO periodicity requires rearranging all charges and spins on a short time scale, a process that typically needs to overcome a high energy barrier. Indeed, our previous work has shown that the SO and CO periodicities remain unchanged even in the “hot-electron”-driven dynamics [8, 23]. Additionally, the “lattice-driven” dynamics in another nickelate family also exhibits no change of SO periodicity [24]. Thus, the observed suppression most likely is due to weakening of the SO and CO diffraction peaks. In this scenario, if the peak width remains unchanged or decreases, the volume of the diffraction peaks also decreases, corresponding to the suppression of order parameter amplitude. If the width increases, depending on the value, the order parameter amplitude may be en-

hanced, remain unchanged, or be suppressed. While the scenario of enhancement is interesting, it appears to be less likely.

The observed behaviors of SO and CO can be described via a Ginzburg-Landau theory. We treat the phonons as an effective driving term on the macroscopic SO and CO, which subsequently reach a “quasi-equilibrium” under the assumption that the electronic order can rearrange sufficiently quickly. We discuss the most likely scenario, where peak positions (*i.e.* periodicity) of SO and CO do not vary. For simplicity, we assume that the correlation length remains unchanged, as in the “hot-electron” dynamics [8, 23]. Hence, the spatial variation of the order parameters can be neglected and the variation of the order parameter amplitude is proportional to the change of peak intensity shown in Fig. 3. We construct a Ginzburg-Landau theory, including terms for the SO, CO, their mutual coupling, and their coupling to lattice distortions, whose free energy is:

$$F = F_o - 2\lambda|S|^2|\rho| + (\alpha|\rho|^2 + \beta|S|^2)u,$$

where  $|\rho|$  and  $|S|$  represent the amplitude of the CO and SO order parameters, respectively.  $F_o = \frac{1}{2}r_\rho|\rho|^2 + |\rho|^4 + \frac{1}{2}r_s|S|^2 + |S|^4$  is the uncoupled Ginzburg-Landau free energy, where the coefficients  $r_\rho$  and  $r_s$  control the thermodynamic stability of the CO and SO.  $\lambda$  is the strength of the coupling between them and the term  $(\alpha|\rho|^2 + \beta|S|^2)u$  describes the lowest-order coupling of the charge and spin stripes to the lattice distortion or phonon  $u$  excited by the pump, with  $\alpha$  and  $\beta$  as the coupling strengths.

Coupling to the lattice distortion changes the landscape of the free energy, reducing the amplitudes of the CO and SO order parameters. The modified amplitudes can be calculated by minimizing  $F$  with respect to  $|\rho|$  and  $|S|$ , where for simplicity we normalize the distortion  $u$  to 1. In addition, we have also set  $\lambda$  to 1 to represent the strongly coupled SO and CO [8, 27, 28]. The values of other parameters are chosen based on thermodynamic properties of the nickelates [8, 20], as also discussed in the Supplemental Material. We note that the particular values do not affect the qualitative behaviors described here.

Since the lattice and charge are expected to couple strongly, we first examine the case where the lattice distortion couples only to the CO (*i.e.*  $\beta = 0$ ). Figure 4(a) shows the effect of coupling on the CO and SO amplitudes, normalized by the amplitudes when  $u = 0$ . The values of all the parameters are detailed in the Supplemental Materials. As expected, increasing the charge-phonon coupling  $\alpha$  suppresses the CO. Although the lattice distortion does not couple to SO directly, the amplitude of SO decreases due to the coupling  $\lambda$ . However, in this case, the SO suppression is always less than that of the CO for all  $\alpha$ . This is inconsistent with our experimental observation in Fig. 3(b), suggesting that the lattice distortion also must couple to SO.

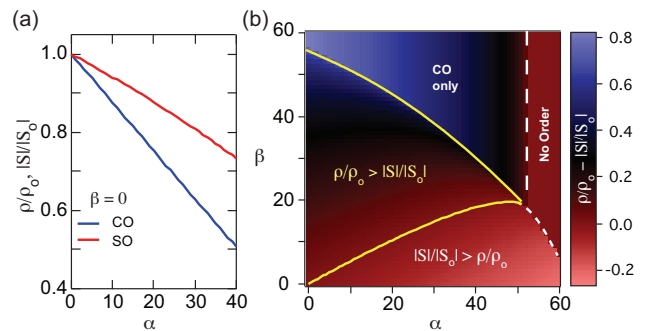


FIG. 4: (color online) (a) Calculated normalized amplitude of the CO and SO order parameters when the lattice distortion couples only to the CO. The amplitude for a given  $\alpha$  is normalized to the amplitudes when  $u = 0$ , *i.e.*  $S_o$  and  $\rho_o$  (b) Stability phase diagram obtained by subtracting the calculated CO and SO amplitudes, *i.e.*  $\rho/\rho_o - |S|/|S_o|$ , as a function of  $\alpha$  and  $\beta$ . The region bounded by yellow solid lines is where SO is affected more by the lattice distortions than CO. The values of all the parameters are detailed in the Supplemental Materials.

If one turns on coupling directly to the SO, the picture changes. The amplitudes of the CO and SO as a function of  $\alpha$  and  $\beta$  are calculated and used to generate a stability phase diagram between the CO and SO amplitude (*i.e.*  $\rho/\rho_o - |S|/|S_o|$ ), as shown in Fig. 4(b). Indeed, the inclusion of a finite SO-lattice coupling  $\beta$  defines a region where  $\rho/\rho_o > |S|/|S_o|$  [the region bounded by yellow solid curves in Fig. 4(b)]. In this region, the CO amplitude is more robust to lattice distortions than the SO amplitude, as seen in experiment. Although this phenomenological model cannot be used to quantify the coupling strengths  $\alpha$  and  $\beta$ , it demonstrates that finite SO-lattice coupling plays an important role in determining the collective behavior of the stripes.

Finally, we discuss the relaxation dynamics. Since the suppression is due to collective coupling to the lattice, the recovery toward equilibrium should be related to the collective modes of SO and CO. As shown in Fig. 3(b), CO relaxation exhibits an exponential behavior with a single time scale of 4 ps. On the other hand, the SO dynamics possesses two time scales: a fast time scale of 2 ps and a slow one that is beyond the time window of the measurement. No coherent oscillations can be resolved, suggesting that the collective modes of CO and SO in striped nickelate are damped, consistent with a recent inelastic neutron scattering result [29]. As in our previous work, we attribute the 4-ps and 2-ps time scales to the recovery of the respective order parameter amplitudes, and the slow dynamics of SO to the recovery of the spin orientation [8, 20, 23].

We emphasize that the “lattice”-driven dynamics qualitatively differs from that of “hot-electrons” generated by optical excitation [8]. First, we do not observe a time scale in the CO dynamics that can be attributed to the

phase dynamics of the order parameter, which was on the order of 10 - 100 ps in the “hot-electron” driven dynamics. Second, in the “hot-electron” dynamics, the CO was always suppressed more than the SO at the same fluence, and the time scales for amplitude recovery were identical between SO and CO due to their mutual coupling. Conversely, for “lattice”-driven dynamics, in the scenario aforementioned, SO is suppressed more than CO, and SO-CO coupling enforces a faster SO amplitude recovery to restore balance with the CO, which we demonstrated in the Supplemental Material.

These results are just the tip of the iceberg, calling for future investigations to elucidate the full SO and CO peak profiles as a function of time, to determine the slow initial suppression time scale, and to measure the lattice dynamics from the time evolution of lattice Bragg peaks. This mode-selective pump-probe methodology for inducing the “lattice”-driven dynamics can be generalized to probe and disentangle subtle interactions in other strongly correlated materials.

We thank Dr. Robert Schoenlein, Dr. Matthew Langner and Dr. Srinivas Raghu for insightful discussions. This research was supported by the Division of Materials Sciences and Engineering of the U.S. Department of Energy, Office of Basic Energy Sciences, under contract DE-AC02-76SF00515 at SLAC National Accelerator Laboratory covering the experimental design, experiment execution, data analysis, and theoretical calculations (W.S.L., B.M., R.G.M., D.H.L., Z.X.S. and T.P.D.), under contract DE-AC02-05CH11231 at Lawrence Berkeley National Laboratory (LBNL) covering RSXS endstation operation (Y.D.C. and Z.H., Advanced Light Source) and covering development of mid-IR excitation at the LBNL (G.C., J.R., and R.A.K., Ultrafast Materials Science program). The use of the Linac Coherent Light Source (LCLS), SLAC National Accelerator Laboratory, is supported by the U.S. Department of Energy, Office of Science, Office of Basic Energy Sciences under Contract No. DE-AC02-76SF00515. Y.F.K. was supported by the Department of Defense (DOD) through the National Defense Science and Engineering Graduate Fellowship (NDSEG) Program and by the National Science Foundation (NSF) Graduate Research Fellowship under Grant No. 1147470. S.G. acknowledges partial support by the Swiss National Science Foundation under fellowship P2EZP2-148737.

---

\* Electronic address: [leews@stanford.edu](mailto:leews@stanford.edu)

† Electronic address: [zxshen@stanford.edu](mailto:zxshen@stanford.edu)

‡ Electronic address: [tpd@stanford.edu](mailto:tpd@stanford.edu)

[1] E. Dagotto, *Science* **309**, 257 (2005).  
 [2] R. J. Cava, B. Batlogg, T. T. Palstra, J. J. Krajewski, W. F. Peck, A. P. Ramirez, and L. W. Rupp, *Phys. Rev. B* **43**, 1229 (1991).

[3] C. H. Chen, S.-W. Cheong, and A. S. Cooper, *Phys. Rev. Lett.* **71**, 2461 (1993).  
 [4] J. M. Tranquada, D. J. Buttrey, V. Sachan, and J. E. Lorenzo, *Phys. Rev. Lett.* **73**, 1003 (1994).  
 [5] A. Vigliante, M. von Zimmermann, J. R. Schneider, T. Frello, N. H. Andersen, J. Madsen, D. J. Buttrey, Doon Gibbs, and J. M. Tranquada, *Phys. Rev. B* **56**, 8248 (1997).  
 [6] C. Schussler-Langeheine, J. Schlappa, A. Tanaka, Z. Hu, C. F. Chang, E. Schierle, M. Benomar, H. Ott, E. Weschke, G. Kaindl, O. Friedt, G. A. Sawatzky, H.-J. Lin, C. T. Chen, M. Braden, and L. H. Tjeng, *Phys. Rev. Lett.* **95**, 156402 (2005).  
 [7] O. Zachar, S. A. Kivelson, and V. J. Emery, *Phys. Rev. B* **57**, 1422 (1998).  
 [8] Y. D. Chuang, W. S. Lee, Y. F. Kung, A. P. Sorini, B. Moritz, R. G. Moore, L. Patthey, M. Trigo, D. H. Lu, P. S. Kirchmann, M. Yi, O. Krupin, M. Langner, Y. Zhu, S. Y. Zhou, D. A. Reis, N. Huse, J. S. Robinson, R. A. Kaindl, R. W. Schoenlein, S. L. Johnson, M. Först, D. Doering, P. Denes, W. F. Schlotter, J. J. Turner, T. Sasagawa, Z. Hussain, Z. X. Shen, and T. P. Devereaux, *Phys. Rev. Lett.* **110**, 127404 (2013).  
 [9] Takashi Hotta and Elbio Dagotto, *Phys. Rev. Lett* **92**, 227201 (2004).  
 [10] S. Yamamoto, T. Fujiwara, and Y. Hatsugai, *Phys. Rev. B* **76**, 165114 (2007).  
 [11] C. C. Homes, J. M. Tranquada, and D. J. Buttrey, *Phys. Rev. B* **75**, 045128 (2007).  
 [12] G. Coslovich, A. F. Kemper, S. Behl, B. Huber, H. A. Bechtel, T. Sasagawa, M. C. Martin, A. Lanzara, R. A. Kaindl *et al.*, arXiv:1603.07819v1  
 [13] J. H. Jung, D.-W. Kim, T. W. Noh, H. C. Kim, H.-C. Ri, S. J. Levett, M. R. Lees, D. McK. Paul, and G. Balakrishnan, *Phys. Rev. B* **64**, 165106 (2001).  
 [14] G. Coslovich, B. Huber, W. -S. Lee, Y. -D. Chuang, Y. Zhu, T. Sasagawa, Z. Hussain, H. A. Bechtel, M. C. Martin, Z. -X. Shen, R. W. Schoenlein and R. A. Kaindl, *Nat. Comm.* **4**, 2643 (2013).  
 [15] A. Subedi, A. Cavalleri, and A. Georges, *Phys. Rev. B* **89**, 220301(R) (2014).  
 [16] J. M. Tranquada, K. Nakajima, M. Braden, L. Pintschovius, and R. J. McQueeney, *Phys. Rev. Lett.* **88**, 075505 (2002).  
 [17] G. Gruner, *Density Waves in Solids* (Westview Press, Cambridge, 2000)  
 [18] M. Le Tacon, A. Bosak, S. M. Souliou, G. Dellea, T. Loew, R. Heid, K-P. Bohnen, G. Ghiringhelli, M. Krisch and B. Keimer, *Nat. Phys.* **10**, 52 (2013).  
 [19] L. Pintschovius, J. M. Bassat, P. Odier, F. Gervais, G. Chevrier, W. Reichardt, and F. Gompf, *Phys. Rev. B* **40**, 2229 (1989).  
 [20] Y.F. Kung, W.-S. Lee, C.-C. Chen, A. F. Kemper, A. P. Sorini, B. Moritz, and T. P. Devereaux, *Phys. Rev. B* **88**, 125114 (2013).  
 [21] C. Bostedt, S. Boutet, D. M. Fritz, Z. Huang, H. J. Lee, H. T. Lemke, A. Robert, W. F. Schlotter, J. J. Turner, and G. J. Williams, *Rev. Mod. Phys.* **88**, 015007 (2016).  
 [22] D. Doering, Y.-D. Chuang, N. Andresen, K. Chow, D. Contarato, C. Cummings, E. Domning, J. Joseph, J.S. Peper, B. Smith, G. Zizka1, C. Ford, W.S. Lee, M. Weaver, L. Patthey, J. Weizeorick, Z. Hussain, P. Denes, *Rev. Sci. Instrum.* **82**, 073303 (2011).  
 [23] W. S. Lee, Y. D. Chuang, R. G. Moore, Y. Zhu, L.

- Patthey, M. Trigo, D. H. Lu, P. S. Kirchmann, O. Krupin, M. Yi, M. Langner, N. Huse, J. S. Robinson, Y. Chen, S. Y. Zhou, G. Coslovich, B. Huber, D. A. Reis, R. A. Kaindl, R. W. Schoenlein, D. Doering, P. Denes, W. F. Schlotter, J. J. Turner, S. L. Johnson, M. Frst, T. Sasagawa, Y. F. Kung, A. P. Sorini, A. F. Kemper, B. Moritz, T. P. Devereaux, D.-H. Lee, Z. X. Shen, and Z. Hussain, *Nat. Commun.* **3**, 838 (2012).
- [24] M. Först, A. D. Caviglia, R. Scherwitzl, R. Mankowsky, P. Zubko, V. Khanna, H. Bromberger, S. B. Wilkins, Y.-D. Chuang, W. S. Lee, W. F. Schlotter, J. J. Turner, G. L. Dakovski, M. P. Minitti, J. Robinson, S. R. Clark, D. Jaksch, J.-M. Triscone, J. P. Hill, S. S. Dhesi and A. Cavalleri, *Nat. Mat.* **14**, 883 (2015).
- [25] T. Katsufuji, T. Tanabe, T. Ishikawa, Y. Fukuda, T. Arima, and Y. Tokura, *Phys. Rev. B* **54**, R14230 (1996).
- [26] M. Först, C. Manzoni, S. Kaiser, Y. Tomioka, Y. Tokura, R. Merlin, and A. Cavalleri, *Nat. Phys.* **7**, 854 (2011).
- [27] R. Kajimoto, K. Ishizaka, H. Yoshizawa, and Y. Tokura, *Phys. Rev. B* **67**, 014511 (2003).
- [28] O. Zachar, S. A. Kivelson, and V. J. Emery, *Phys. Rev. B* **57**, 1422 (1998).
- [29] S. Anissimova, D. Parshall, G.D. Gu, K. Marty, M.D. Lumsden, Songxue Chi, J.A. Fernandez-Baca, D.L. Abernathy, D. Lamago, J.M. Tranquada and D. Reznik, *Nat. Commun.* **5**, 3467 (2014).